2023 IEEE International Conference on Robotics and Automation (ICRA 2023)
May 29 - June 2, 2023. London, UK

Strained Elastic Surfaces with Adjustable-Modulus Edges (SESAMEs) for Soft Robotic Actuation

Christopher J. Kimmer[1], Michael Seokyoung Han[2], and Cindy K. Harnett[3]

***Abstract*— For robots to interact safely with humans and travel with minimal weight, low-density packable actuators are sought. Electronically-driven active materials like shape memory wire and other artificial muscle fibers offer solutions, but these materials need a restoring force. Moreover, if joint bending is required, the actuators must exert a bending moment around the joint. In this paper, we model the three-dimensional shapes of strained elastic surfaces with adjustable-modulus edges (SESAMEs), then implement SESAMEs by machine embroidering shape memory alloy wire onto stretched elastic fabric, showing a path to lightweight actuators that exert bending forces and have built-in restoring forces. SESAMEs start out planar, and upon release from the plane take on three-dimensional shapes thanks to the balance between bending energy in the boundary and strain energy in the elastic surface. The elastic creates both a restoring force to bring the boundary back to its original shape after actuation, and an out-of-plane structure for applying a bending moment. We demonstrate SESAMEs' properties as soft robotic actuators individually and in arrays, and coupled to flexible plastic frames during the planar fabrication process as bending actuators to switch bistable mechanical structures.**

I. Introduction

Actuators that can exert bending forces are plentiful in the natural world, making insect joints move and plant stems curl. These systems typically operate by differential expansion of one layer relative to another, caused by swelling or shrinking of cells driven by biological signals [1], [2]. Soft robotics researchers have taken cues from nature, developing a wide variety of inflatable actuators [3]–[5]. But because pressure sources add bulk and complexity, there is an ongoing search for electronically-driven actuator systems, including shape memory materials, liquid crystal elastomers, and dielectric elastomer actuators. Most of these efforts originate with wires or foils and films that are shaped into three-dimensional (3D) actuators by embedding wires into sheets wrapped around objects [6], cutting and applying foils [7], or layered 3D printing of active materials [8], [9]. Other technologies such as dielectric elastomer actuators made from thin films stretched on frames [10] use stress integrated during fabrication to produce final 3D shapes that can apply bending moments to other structures. This paper is in the latter category: we attach a stretched elastic fabric to a frame that is initially planar, but when released from the surface, responds to the elastic forces by bending. Unlike dielectric elastomer actuators, where the focus is on changing the tension of the stretched film by applying an electric field, our focus is on changing the elastic modulus of the boundary.

A high-modulus boundary resists bending, staying flat and keeping the elastic film stretched. A low-modulus boundary bends, allowing the elastic to shrink back toward its original length. Materials such as shape memory alloy wire, shape memory polymer, drawstrings and tendons, and jamming structures such as beads on a string, all have an effective modulus that one can adjust to reprogram the shape of these structures. This paper first discusses the general problem of shape-finding for these structures, then implements them using shape memory wire embroidered around the edge of strained elastic fabric (Fig. 1) and investigates their force production, bending, and curvature-changing properties.

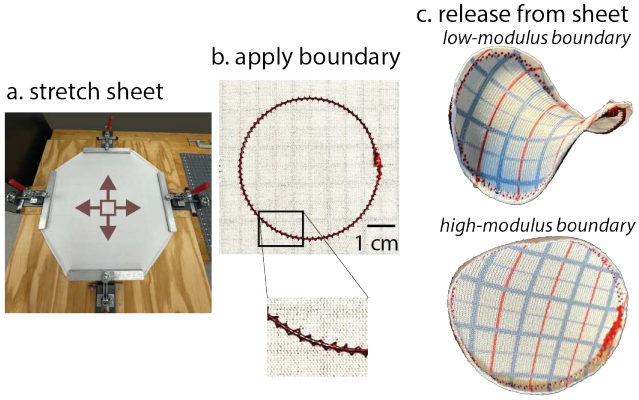

Fig. 1. a. Stretching, b. framing, and c. release of SESAME surfaces with low and high elastic modulus materials for the boundary.

Much of the interplay between the energetics of a stretched surface and a flexible boundary can be described using idealized models. Giomi and Mahadevan [11] studied soap films bounded by a flexible boundary empirically, analytically, and computationally. They consider a soap film spanning a flexible boundary of fixed length characterized by the surface tension of the film, length of the boundary, and its bending rigidity. A single dimensionless parameter describes the ratio of surface tension to bending rigidity normalized by the length. For small value of this parameter, the surface energy is much less than the boundary energy, and a flat surface spans the constant-curvature, circular boundary. At

This work is supported by U. S. National Science Foundation grant 1935324, EFRI C3 SoRo: Control of Local Curvature and Buckling for Multifunctional Textile-Based Robots.

[1]C. J. Kimmer is with Informatics, School of Natural Science, Indiana University Southeast, New Albany, IN, US cjkimmer@ius.edu

[2]M. S. Han is with the Department of Mechanical Engineering, University of Louisville, Louisville, KY USA seokyoung.han@louisville.edu

[3]C. K. Harnett is with the Department of Electrical and Computer Engineering, University of Louisville, Louisville, KY USA c0harn01@louisville.edu

the other extreme with surface energy dominating the boundary energy, the boundary is elongated and the equilibrium shape has buckled to exhibit out-of-plane deformation. Chen and Fried [12] carried out a stability and buckling analysis for this system. Majid [13] considered the same system with a different numerical approach and also observed a transition from planar to out-of-plane deformation as well as a regime where self-intersecting solutions occur as the boundary increasingly bends out of plane.

Giusteri et al. [14] study the so-called Kirchhoff-Plateau problem and considered a soap film with boundary described by the midline of a Kirchhoff rod. In this system the boundary energy contains both bending and twisting terms, and they prove the existence of energy-minimizing solutions. Biria and Fried [15] characterize the buckling modes of this Kirchhoff-Plateau system as its energetics vary. The addition of boundary twist energy introduces a second dimensionless parameter characterizing the system and an additional buckling mode with a twisted boundary when the torsional rigidity of the boundary is small relative to the bending rigidity.

However, soap films differ from the strained elastic materials presented here. Perez studied Kirchhoff-Plateau surfaces based on fabrics [16], describing bending of 3D printed plastic lines that support stretched fabrics. Others in the realm of architecture and design have created pop-up 3D structures by similar means. Most are static shapes, but a few have investigated thermal shape memory materials as *4D* methods to evolve the 3D shape as conditions change [17], [18]. These studies are the closest to the SESAME concept presented here, where 3D shapes evolve by adjusting the mechanical properties of the bounding frame instead of changing the surface tension.

Others have made active Kirchhoff-Plateau type surfaces using a passive boundary and changeable membrane stress. Researchers have stretched acrylic elastomers over open frames, including flexible frames cut from thin materials that easily bend out of plane. The balance between strain energy in the elastomer and bending energy in the flexible frame produces three-dimensional (3D) shapes. When the effective surface tension of the membrane is reduced by applying electric fields to squeeze the membrane, the membrane increases its surface area and the 3D shape flattens, relieving its bending energy. This programmable surface tension produces flapping motions and bending motions with a large displacement. Compared to linear actuators, including shape memory alloy springs embedded in fabrics [19] and soft linear actuators such as coiled polymer fibers [20], [21], the shapes and actuation paths here are complex. However, dielectric elastomer actuator projects have laid some groundwork for making practical actuators from these 3D energy-minimizing shapes. Design lessons from the architectural form-finding community are likely to apply to our work too.

Here we emphasize planar-to-3D construction using textile fabrication methods instead of 3D printing or gluing films to laser-cut frames. The advantages are mainly in speed, automation, and availability of new materials that don't work with those methods. In this work, an industrial machine ties the boundary to the elastic material without the adhesive requirements of dielectric elastomer fabrication or the printability requirements of 3D printed boundary methods. Architectural researchers have used a similar industrial embroidery machine for tailored fiber placement in pre-strained elastic producing 3D structures by patterning carbon fiber and then infiltrating it with epoxy to selectively stiffen paths in the elastic. When released, the 2D structure went out of plane to produce dome-like and negative curvature shapes governed by the fiber layout pattern [22].

The boundary material we use to demonstrate the SESAME concept is shape memory alloy (SMA) wire. We rely on its modulus change with temperature, rather than aiming to recover a specific trained shape upon heating. Its as-received trained shape is a straight line. In our previous work [23], this material was coupled with other elastic bendable surfaces to control shapes by changing local curvature.

First we investigate the scaling rules for achieving 3D shapes from a basic SESAME cell: a circular boundary spanned by a stretched elastic film. Then, scaling rules are tested by fabricating and measuring individual and arrayed SESAMEs, and finally, their actuation properties are evaluated alone and coupled with flexible plastic beams to drive a multistable structure.

II. Methods

A. Modeling And Validation

Simulation is used to explore the design space of a single strained fabric and SMA wire SESAME actuator. We model it as an elastic sheet spanning a flexible boundary. Since the thickness of the fabric is much less than its other dimensions, it is treated as a plate whose energy contains separate stretching and bending terms [24]. The fabric's bending energy is proportional to the square of its mean curvature, H, while its stretching energy depends on its constitutive model. We treat the fabric as a St. Venant-Kirchoff hyperleastic material, a good compromise between simplicity and accuracy when modeling the mechanics of textiles [25]. The fabric's stretching energy then depends on its Young's modulus E_f, thickness t, Poisson's ratio ν, and the Green-Lagrange strain $\mathbf{E}$. The resulting energy functional is given by

$$E_f t \int \mathrm{d}A f(\mathbf{E}) + \frac{E_f t^3}{6(1-\nu^2)} \int H^2 \mathrm{d}A + \frac{1}{2} E_w I_w \oint \kappa^2 \mathrm{d}l \tag{1}$$

where the third term describes the bending energy of a boundary wire having a circular cross section, path curvature κ, modulus E_w, radius r_w, and moment $I_w = \pi r^4/4$. The strain energy density for the fabric is

$$f(\mathbf{E}) \equiv \frac{1}{1+\nu} \left(Tr(\mathbf{E}^2) + \frac{\nu}{1-2\nu} (Tr\mathbf{E})^2 \right). \tag{2}$$

The flexible but inextensible boundary is subject to the length constraint

$$\oint \mathrm{d}l = L \tag{3}$$

which is enforced by a Lagrange multiplier and in practice adds a stretching energy term for the wire boundary. The fabric thickness t is $\ll L$.

We use a dimensionless form of Equation 1

$$\int \mathrm{d}A f(\mathbf{E}) + \alpha \int H^2 \mathrm{d}A + \beta \oint \kappa^2 \mathrm{d}l. \tag{4}$$

α depends on geometric and material properties of the fabric and is given by $t^2/6L^2(1-\nu^2)$. $\beta = E_w I_w / 2E_f t L^3$ is the ratio of wire to surface moduli and is thus analogous to the reciprocal of the dimensionless parameter in [11]. Large β means the boundary stiffness dominates, while small β means the elastic sheet can easily bend the boundary.

The Surface Evolver [26] is used to minimize the energy in Eq. 4 for each geometric configuration. This software was chosen because of its capability of modeling both mechanical and geometrical energy functionals while having built-in mesh refinement capabilities. With the Surface Evolver we model systems with elliptical wire boundaries parameterized by the eccentricity of the elliptical boundary and the parameter β. The reference configuration for each modeled SESAME actuator is a homogeneously strained fabric surrounded by a flexible, circular boundary in the x-y plane. A 2D homogeneous strain is applied to stretch the system uniformly in plane and random small displacements are applied to the boundary out of plane. The elliptical wire boundary is discretized into 20 segments which are each joined by edges to the centroid of the ellipse to generate the initial triangulation. This coarse initial triangulation is refined twice by subdividing each triangle into 4 smaller triangles with vertices added at each edge's centroid. After refinement, the energy of the system is minimized, and this refinement followed by minimization cycle can be repeated until the desired level of convergence is reached.

B. Fabrication

1) Shape memory alloy wire: Shape memory alloy (SMA) wire was obtained from Nexmetal.com (Nitinol SMA Muscle Wire, Nexmetal Corporation, Cheyenne, WY USA) with a range of transition temperatures between the martensite and austenite phase. A general rule is that the modulus of the low-temperature martensite phase of Nitinol is about 1/3 that for the high temperature austenite phase. We used values of 28 GPa for martensite and 75 GPa for austenite [27]. Since SMA is difficult to solder, we made connections between SMA and power wires by mechanical compression of thin-walled crimp tubes.

2) Textile fabrication: To verify uniformity of stretching, elastic fabric was printed with a 1 cm grid having 5 mm sub-increments, with red lines along the ribs of the knit (Sport Lycra, Spoonflower Inc., Durham NC, USA). We measured the modulus of the fabric using a spring scale and ruler, taking an average of the result in two orthogonal directions, and using a micrometer to measure the thickness of five stacked layers. All devices were made from the same kind of fabric. Fabric properties are detailed in Table I. Fabric pieces were stretched biaxially using four silkscreen stretchers as shown in Fig. 1a, then captured on a magnetic hoop (Mighty Hoop, Midwest Products, Inc., Germantown, Wisconsin, USA) taped to a water-soluble film (Vilene, Freudenberg Performance Materials, Weinheim, Germany) that was clamped in the pantograph of an industrial embroidery system (JCZA, ZSK Stickmaschinen GmbH, Krefeld, Germany) with a tailored wire placement head that dispensed SMA wire along computer-controlled paths.

3) Bending beam fabrication: Elastic beams and constraining beams were produced by cutting 0.015" (0.38 mm) thick polycarbonate sheets on a computer-controlled cutting machine (ScanNCut, Brother International Corporation). Beams were connected to constraints and to other beams using plastic rivet snaps.

C. Methods for testing SESAME properties

- **3D scans** The SESAME surfaces' three-dimensional shapes were scanned using photogrammetry software (ScandyPro app, ScandyCo, Louisiana, USA).
- **Surface temperatures** were measured using an infrared camera (E6 infrared camera, Teledyne FLIR LLC).
- **Joule heating** of SMA wire was carried out using a DC benchtop supply at voltages up to 18V and currents up to 3A.
- **In-plane force testing** was done with a 20 N load cell (Nextech Global Co., Ltd.) with the sensor and load cell attached to an optical breadboard. Blocking forces were measured following the procedure of Fig 3 in [10].
- **Out-of-plane displacement** was measured by video analysis. Different loads were added to an acrylic slab on top of 2D SESAME arrays during Joule heating, and we measured the height of the underside of the slab above the support surface.
- **Cyclic actuation** of bending segments was managed by a microcontroller board (Arduino Uno) sending digital signals to drive DC currents of up to 3A through NPN transistors (TIP 120).

III. Design and Implementation

A. Modeling

We have minimized Eq. 4 for a range of systems with circular boundaries and boundary flexural rigidities as described above. We vary the parameter β from 0.01 to 0.25 in increments of 0.01, and the fabric strain ϵ from 0 to 0.5 in increments of 0.02. Flat systems remain in the x-y plane, so the difference Δz between the maximum and minimum z-component of boundary vertices provides a useful measure of whether or not the system has buckled out of plane. Fig. 2a shows Δz as a function of β and ϵ. As β increases, more initial strain is required if the system is to buckle out of plane. All the buckled systems computed in this manner are qualitatively similar to the one shown in Fig. 2b. For small β and large strain, there is little resistance to bending from the compliant boundary, and the surface may self-intersect

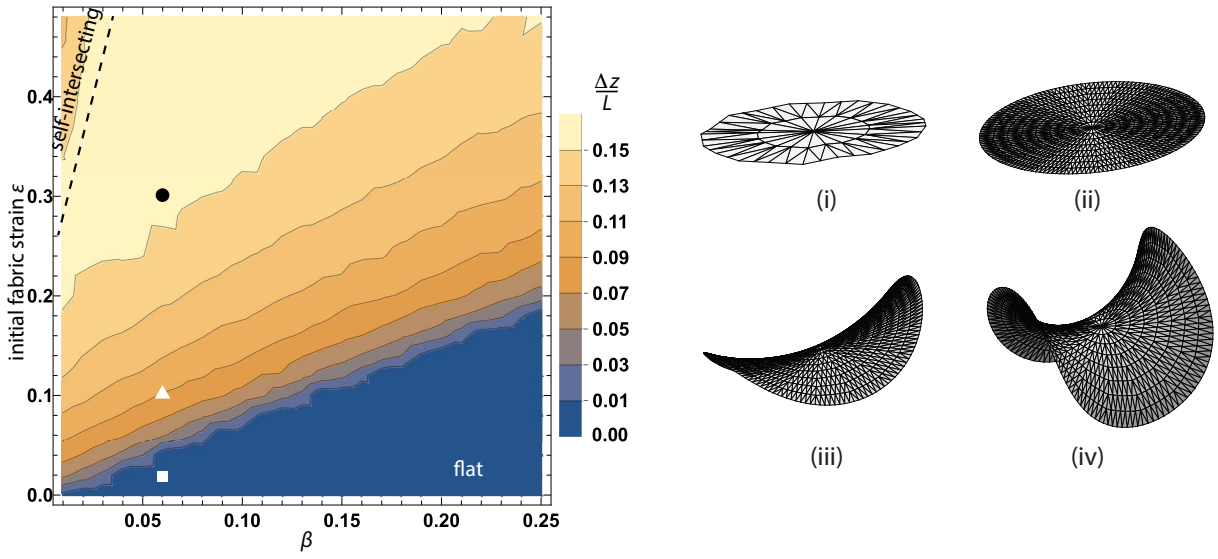

Fig. 2. Left: Contour plot of the boundary wire height vs β and the initial strain ϵ. The circle, triangle, and square are for SESAME actuators with $\beta = 0.06$. The black circle has strain $\epsilon = 0.3$ and corresponds to the actuators fabricated in this work. Right: Initial (i) and minimized triangulations for a system with $\epsilon = 0.02$ (ii, white square), 0.1 (iii, white triangle), and 0.3 (iv, black circle).

as its energy is minimized. The Surface Evolver does not prevent this unphysical behavior, and the small region of this behavior is indicated in Fig. 2.

In general, systems with greater initial strain exhibit more curvature and thus a higher bending energy and larger Δz than those with smaller strains. Heating SMA-wire bounded structures increases the boundary stiffness, increases β, and leads to a flatter structure. For the systems fabricated in this work, heating roughly triples the value of β and leads to a smaller but nonzero Δz. Fig. 2 indicates that systems with smaller initial strain could flatten completely upon heating due to this increase in β.

B. SESAME Implementations

SESAMEs were constructed as individual loops (Fig. 1c) and as two-dimensional arrays for measuring out-of-plane forces. Lateral forces from a single loop were measured, and arrays of SESAMEs were sandwiched around flexible plastic beams for a bending actuator demonstration.

1) SESAME Arrays: Arrays of SESAMEs were created using the method of Fig. 3a to produce a continuous electrical path through a grid of circles. Polyester threads covered the first half of the path in Fig. 3a prevented the junctions from shorting out; refer to the inset in Fig. 1b for details. SESAME arrays started out planar (Fig. 3b), and upon release and removal of the water-soluble film, took on a 3D shape that kept tangent edges of neighboring SESAMEs parallel (Fig. 3c). To study the scaling of SESAME structures, two types of structures were created (Table I) using the same 30% biaxially strained fabric. *Large* structures used thick wire, and *small* had thinner wire. Keeping the ratio β constant by adjusting the SESAME diameter led to similar 3D shapes for the *large* (Fig. 3 b,d,f) and *small* (Fig. 3 c,e,g) designs at different size scales.

TABLE I
PROPERTIES OF FABRICATED SESAME ARRAYS

Property	*large* array	*small* array
Fabric strain ϵ	0.3	same
Fabric Thickness t (mm)	0.27	same
Fabric Modulus E_f (kPa)	700	same
Wire Modulus E_w **at 25°C** (GPa)	28	same
SMA Transition Temp. (°C)	40	60
Loop Diameter d_0 (cm)	5.0	2.5
Wire Diameter d_w (mm)	0.5	0.3

When calculating the ratio β of bending energy to strain energy, we considered the elastic modulus E_w to be similar for both types of wire in Table I at the low end of the temperature range, below the transition temperature for both materials. Both types of structure also used the same fabric and strain, so preserving β meant preserving I/L^3. For circular loops of diameter d_0, constant d_w^4/d_0^3 will keep β constant in the same strained fabric for the same boundary material. A loop diameter d_0 of 2.5 cm was thereby calculated to make *small* structures of 0.3 mm diameter wire have 3D shapes similar to *large* ones made with 0.5 mm diameter wire and d_0 = 5 cm. Measurements of the resulting array heights h from scans in Fig. 3f and Fig. 3g produced a height-to-loop perimeter $h/\pi d_0$ ratio of 0.14 for *small* structures and 0.15 for *large* structures, indicating good similarity. These results are close to the value of 0.154 given by the model (black dot on Fig. 2a).

2) Out-of-Plane Actuation with 2-D Arrays: Vertical forces exerted by two-dimensional arrays were investigated

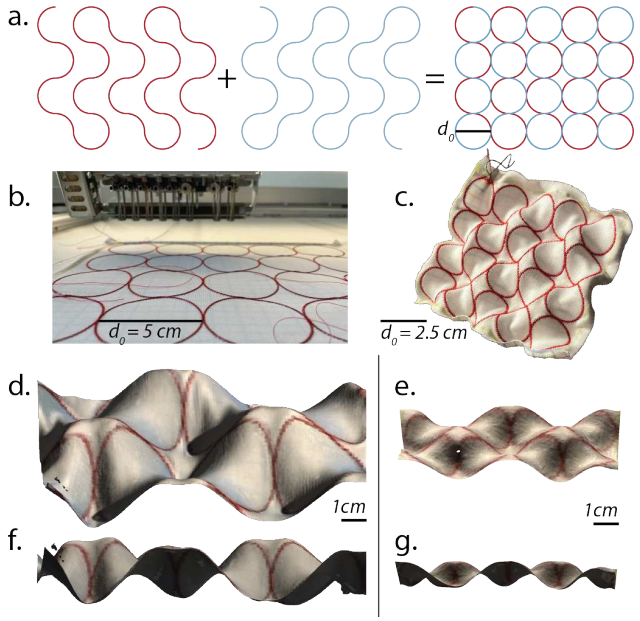

Fig. 3. a. Layout for single-circuit SESAME arrays. b. A 5cm diameter *large* array before releasing from the hoop. c. Photo of a 2.5 cm diameter *small* array after release. d-g Orthographic perspective 3D scans of fabricated arrays at 25°C: d. *large* structure overview, e. *small* structure overview, f. *large* structure cross-section, g. *small* structure cross-section

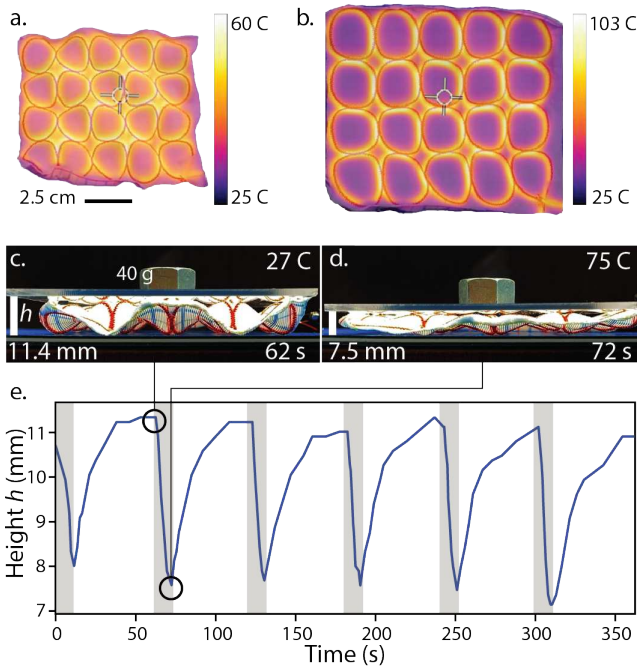

Fig. 4. Implementation of a 2-D SESAME array for out-of-plane actuation. a. Low-temperature and b. high-temperature states. c. A low temperature array supports a weight; maximum wire temperature is shown d.Heated array lowers the weight. e. Height during cyclic application of 0.9 A heating current at intervals indicated by gray bars.

for out-of-plane lifting (Fig. 4). Here, the *small* array design of Table I and Fig. 3c was covered with a weighted acrylic slab (40 g, compared to the array's 3.9 g weight) and heated by cyclic current as displacement was monitored. More than 50 percent of the height was recovered in the first ten seconds after removing the current.

3) Lateral blocking force from a single loop: In-plane lateral forces are useful for creating bending and fast snapping motions. When neighboring SESAME cells push against each other, a SESAME array will expand laterally, and if tethered to a flexible but inextensible surface, the surface will curl to permit the expansion. To investigate these lateral forces, we evaluated the force exerted by a single *large* SESAME actuator in Fig. 5, clamping it between a plate and a force gauge with a fixed 2 cm distance slightly smaller than its natural room-temperature saddle shape as illustrated in the Fig. 5 side-view inset. With a 1.3 A applied current, the force approached 0.5 N over a period of 45 seconds. Slow speed is a typical issue for SMA applications. The force dropped rapidly when the current was removed, likely due to heat sinking of the saddle tips where they contacted the plate and underlying table. Careful control of the SMA thermal environment can increase actuation speed [28], and so can connecting actuators to snapping and buckling mechanical structures [29].

4) SESAMEs as Bistable Beam Benders: To demonstrate bending motions originating from lateral forces, we sandwiched a plastic beam between a pair of linear SESAME arrays as illustrated in Fig. 6a. Because forces were desired only along the beam direction, we used the embroidery

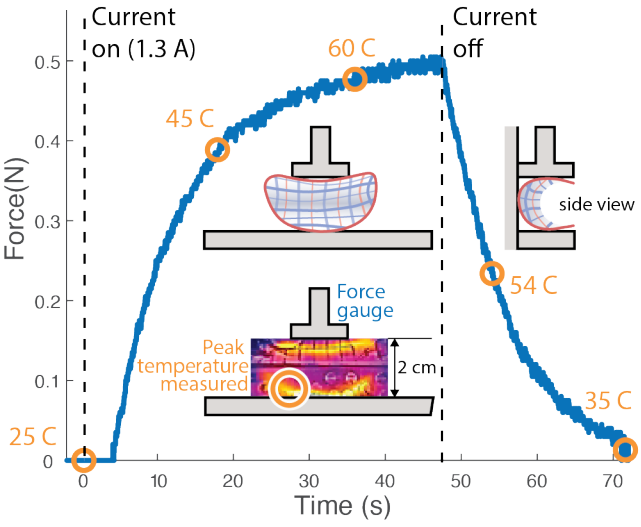

Fig. 5. Blocking force at 2cm for a single SESAME loop made from 0.5 mm diameter SMA wire with a 40 C transition temperature in a 30 percent prestrained elastic fabric sheet with 5cm loop diameter.

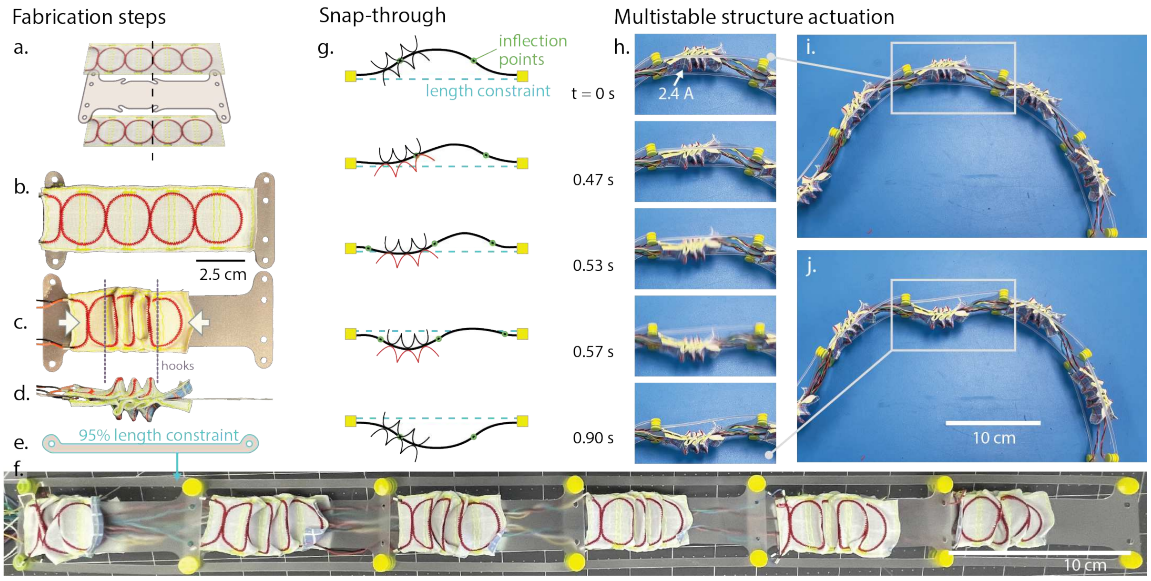

Fig. 6. Bistable segments store mechanical energy from SESAME bending actuators. a: Fabrication using planar embroidery methods, b-f assembly into bistable segments with inflection-point actuators, g. Snap-through curvature propagation mechanism, h. snap-through of a single segment in a chain.

machine to put a stripe of inextensible thread across the center of each loop, preventing excessive sideways expansion during heating. The sandwich was built on the embroidery machine pantograph by putting an array of plastic beams on top of a newly-sewn SESAME array, then applying a previously-made SESAME array that was left clamped in a hoop. Aligning everything in the flat state allowed the machine to tie the opposing SESAMEs at their edges (yellow stitching in Fig. 6b), creating an array of six beams with SESAME sleeves. The sleeves were compressed to catch on hooks (Fig. 6c) constraining actuation to one half of the beam, as shown in the side view (Fig. 6d), and squeezing the structures to a narrower width than the elastic material produced alone. Bistable structures were formed by attaching length constraints to the beams (Fig. 6e) using plastic rivet snaps. These snaps were also used to join the segments in an array (Fig. 6f) producing a multisegment structure modeled on a design from our earlier work, which showed how to form arbitrary 2D shapes from chains of bistable curved elements [30]. When the SESAME on the concave side of a segment was heated, it expanded and caused snap-through by changing an inflection point to a local curvature maximum (Fig. 6g). Segments were supplied with 2.4 A for approximately 1 second and powered off when they attained the new state, reaching a maximum temperature of 65 C on the powered side and 35 C on the unpowered side. Powering the opposite side actuator put it back in the original state. The bistable structure generated fast (40 cm/s) motions during snap-through and captured energy injected into the system during heating.

IV. Discussion and Conclusions

In this work we investigated scaling of strained elastic sheets with compliant boundaries, developing a model based on the parameter β, the ratio of boundary to elastic membrane moduli. The model was useful in scaling the actuator diameter to achieve self similar shapes for two different boundary wire diameters, even though it did not account for boundary twisting or the anisotropic elastic modulus of the stretched fabric membrane (in this case, differing by 10 percent in two orthogonal directions). We achieved out-of-plane and in-plane actuation by adjusting the boundary modulus during runtime, demonstrated a SESAME array lifting more than 10 times its weight, and applied the concept in a bistable beam bending demonstration. Bistable and multistable structures are emerging in soft robotics for multiple reasons: their ability to retain a reconfigured shape without power, their high peak forces and their fast snapping motions [29], [31]–[36]. Designs are often inspired by plants that couple cellular swelling with elastic properties [1], [37], [38].

For these demonstrations, the boundary was SMA wire. While SMA wire is easy to interface, it has high power consumption and low bandwidth. Other methods to create variable-modulus elastic lines could improve performance. These include 1-D tendon-based jamming, other thermally driven materials with phase transitions such as liquid crystal elastomers and shape memory polymers in fiber formats, liquid metal filled channels, and tubes with variable fluid pressure. These flexible filaments would likely work with the textile fabrication method used in this paper, which can pattern materials up to a few millimeters in diameter. Other modifications, like inextensible threads to control expansion, will help tune the speed, force, and direction of these actuators. A key advantage of this type of strain engineering is the convenience and speed of building devices in a planar format, only going 3D at the final release step.

REFERENCES

[1] Shahaf Armon, Efi Efrati, Raz Kupferman, and Eran Sharon. Geometry and mechanics in the opening of chiral seed pods. *Science*, 333(6050):1726–1730, September 2011.

[2] Suyi Li and K W Wang. Plant-inspired adaptive structures and materials for morphing and actuation: a review. *Bioinspir. Biomim.*, 12(1):011001, December 2016.

[3] Y Sun, Y S Song, and J Paik. Characterization of silicone rubber based soft pneumatic actuators. *2013 IEEE/RSJ International*, 2013.

[4] Benjamin C Mac Murray, Xintong An, Sanlin S Robinson, Ilse M van Meerbeek, Kevin W O'Brien, Huichan Zhao, and Robert F Shepherd. Poroelastic foams for simple fabrication of complex soft robots. *Adv. Mater.*, 27(41):6334–6340, November 2015.

[5] R Niiyama, D Rus, and S Kim. Pouch motors: Printable/inflatable soft actuators for robotics. In *2014 IEEE International Conference on Robotics and Automation (ICRA)*, pages 6332–6337. ieeexplore.ieee.org, May 2014.

[6] S Y Kim and R Kramer-Bottiglio. Roboticizing fabric by integrating functional fibers. *Proceedings of the National Academy of Sciences*, 117(41):25360–25369, 2020.

[7] E Hawkes, B An, N M Benbernou, H Tanaka, S Kim, E D Demaine, D Rus, and R J Wood. Programmable matter by folding. *Proc. Natl. Acad. Sci. U. S. A.*, 107(28):12441–12445, July 2010.

[8] Shuo Li, Hedan Bai, Zheng Liu, Xinyue Zhang, Chuqi Huang, Lennard W Wiesner, Meredith Silberstein, and Robert F Shepherd. Digital light processing of liquid crystal elastomers for self-sensing artificial muscles. *Sci Adv*, 7(30), July 2021.

[9] Binjie Jin, Jiaqi Liu, Yunpeng Shi, Guancong Chen, Qian Zhao, and Shu Yang. Solvent-assisted 4D programming and reprogramming of liquid crystalline organogels. *Adv. Mater.*, 34(5):e2107855, February 2022.

[10] G Kofod, M Paajanen, and S Bauer. Self-organized minimum-energy structures for dielectric elastomer actuators. *Appl. Phys. A: Mater. Sci. Process.*, 85(2):141–143, November 2006.

[11] L Giomi and L Mahadevan. Minimal surfaces bounded by elastic lines. *Proceedings of the Royal Society A: Mathematical, Physical and Engineering Sciences*, 468(2143):1851–1864, July 2012.

[12] Yi-Chao Chen and Eliot Fried. Stability and bifurcation of a soap film spanning a flexible loop. *J. Elast.*, 116(1):75–100, June 2014.

[13] Abdul Majid. Simulation of a soap film spanning a flexible loop. *International Journal of Non-Linear Mechanics*, 124:103497, 2020.

[14] Giulio G Giusteri, Paolo Franceschini, and Eliot Fried. Instability paths in the kirchhoff–plateau problem. *J. Nonlinear Sci.*, 26(4):1097–1132, August 2016.

[15] Aisa Biria and Eliot Fried. Buckling of a soap film spanning a flexible loop resistant to bending and twisting. *Proceedings of the Royal Society A: Mathematical, Physical and Engineering Sciences*, 470(2172):20140368, 2014.

[16] Jesús Pérez, Miguel A Otaduy, and Bernhard Thomaszewski. Computational design and automated fabrication of kirchhoff-plateau surfaces. *ACM Trans. Graph.*, 36(4):1–12, July 2017.

[17] Kycia, Agata, Guiducci, and Lorenzo. Self-shaping textiles - a material platform for digitally designed, material-informed surface elements. *Proceedings of 38th Education and Research in Computer Aided Architectural Design in Europe (eCAADe) Conference, Berlin (Online)*, 2020.

[18] H C Koch, D Schmelzeisen, and T Gries. 4D textiles made by additive manufacturing on pre-stressed textiles—an overview. *Actuators*, 2021.

[19] Seong Jun Park, Uikyum Kim, and Cheol Hoon Park. A novel fabric muscle based on shape memory alloy springs. *Soft Robot*, 7(3):321–331, June 2020.

[20] Carter S Haines, Márcio D Lima, Na Li, Geoffrey M Spinks, Javad Foroughi, John D W Madden, Shi Hyeong Kim, Shaoli Fang, Mônica Jung de Andrade, Fatma Göktepe, Özer Göktepe, Seyed M Mirvakili, Sina Naficy, Xavier Lepró, Jiyoung Oh, Mikhail E Kozlov, Seon Jeong Kim, Xiuru Xu, Benjamin J Swedlove, Gordon G Wallace, and Ray H Baughman. Artificial muscles from fishing line and sewing thread. *Science*, 343(6173):868–872, February 2014.

[21] Jiefeng Sun, Brandon Tighe, Yingxiang Liu, and Jianguo Zhao. Twisted-and-Coiled actuators with free strokes enable soft robots with programmable motions. *Soft Robot*, 8(2):213–225, April 2021.

[22] Lotte Aldinger, Georgia Margariti, Axel Körner, and Jan Knippers. Tailoring Self-Formation:fabrication and simulation of membrane-actuated stiffness gradient composites. In *Proceedings of the IASS Symposium 2018 - Creativity in Structural Design*, pages Vol. 2018, No. 18, pp. 1–8. International Association for Shell and Spatial Structures (IASS), July 2018.

[23] Paul Bupe, Douglas J Jackson, and C K Harnett. Electronically reconfigurable virtual joints by shape memory Alloy-Induced buckling of curved sheets. In *IEEE SoutheastCon*, pages 598–604, March 2022.

[24] Lev Davidovich Landau and Evgenij M Lifšic. *Theory of elasticity: volume 7*, volume 7. Elsevier, 1986.

[25] Pascal Volino, Nadia Magnenat-Thalmann, and Francois Faure. A simple approach to nonlinear tensile stiffness for accurate cloth simulation. *ACM Transactions on Graphics*, 28(4):Article–No, 2009.

[26] Kenneth A Brakke. The surface evolver. *Experimental mathematics*, 1(2):141–165, 1992.

[27] Sung-Hyuk Song, Jang-Yeob Lee, Hugo Rodrigue, Ik-Seong Choi, Yeon June Kang, and Sung-Hoon Ahn. 35 hz shape memory alloy actuator with bending-twisting mode. *Sci. Rep.*, 6:21118, February 2016.

[28] Xiaonan Huang, Kitty Kumar, Mohammad K Jawed, Amir Mohammadi Nasab, Zisheng Ye, Wanliang Shan, and Carmel Majidi. Highly dynamic shape memory alloy actuator for fast moving soft robots. *Advanced Materials Technologies*, 4(4):1800540, 2019.

[29] Yichao Tang, Yinding Chi, Jiefeng Sun, Tzu-Hao Huang, Omid H Maghsoudi, Andrew Spence, Jianguo Zhao, Hao Su, and Jie Yin. Leveraging elastic instabilities for amplified performance: Spine-inspired high-speed and high-force soft robots. *Science Advances*, 6(19):eaaz6912, 2020.

[30] C K Harnett and C J Kimmer. Digital origami from geometrically frustrated tiles. In *ASME 2013 International Design Engineering Technical Conferences and Computers and Information in Engineering Conference*, pages V06BT07A046–V06BT07A046. American Society of Mechanical Engineers, August 2013.

[31] Lishuai Jin, Yueying Yang, Bryan O Torres Maldonado, Sebastian David Lee, Nadia Figueroa, Robert J Full, and Shu Yang. Ultra-fast, programmable, and electronics-free soft robots enabled by snapping metacaps. October 2022.

[32] Yinding Chi, Yanbin Li, Yao Zhao, Yaoye Hong, Yichao Tang, and Jie Yin. Bistable and multistable actuators for soft robots: Structures, materials, and functionalities. *Adv. Mater.*, 34(19):e2110384, May 2022.

[33] Tian Chen, Osama R Bilal, Kristina Shea, and Chiara Daraio. Harnessing bistability for directional propulsion of soft, untethered robots. *Proceedings of the National Academy of Sciences*, 115(22):5698–5702, 2018.

[34] Shuzhen Wei and Tushar K Ghosh. Bioinspired bistable dielectric elastomer actuators: Programmable shapes and application as binary valves. *Soft Robot*, 9(5):900–906, October 2022.

[35] Dinesh K Patel, Xiaonan Huang, Yichi Luo, Mrunmayi Mungekar, M Khalid Jawed, Lining Yao, and Carmel Majidi. Highly dynamic bistable soft actuator for reconfigurable multimodal soft robots. *Adv. Mater. Technol.*, page 2201259, November 2022.

[36] Zechen Xiong, Liqi Chen, Wenxiong Hao, Pengfei Yang, Shicheng Wang, Sarah Li Wilkinson, Yufeng Su, Xiangyi Ren, Nipun Poddar, Xi Chen, and Hod Lipson. In-plane prestressed hair clip mechanism for the fastest untethered compliant fish robot. July 2022.

[37] Yoël Forterre, Jan M Skotheim, Jacques Dumais, and L Mahadevan. How the venus flytrap snaps. *Nature*, 433(7024):421–425, January 2005.

[38] Peter Fratzl, Rivka Elbaum, and Ingo Burgert. Cellulose fibrils direct plant organ movements. *Faraday Discuss.*, 139:275–82; discussion 309–25, 419–20, 2008.